Measurement of ^{63,65}Cu$(n,\gamma)^{64,66}$Cu and ^{59}Co$(n,\gamma)^{60}$Co Maxwellian-averaged neutron-capture cross sections

L. Weissman,[1,*] M. Tessler,[1] A. Barak,[1] H. Dafna,[1] A. Grin,[1] B. Kaizer,[1] D. Kijel,[1] A. Kreisel,[1] M. Paul,[2] A. Perry,[1] I. Silverman,[1] N. Tamim,[1] and T. Zchut[1]

[1]*Soreq Nuclear Research Center, Yavne 81800, Israel*

[2]*Hebrew University, Jerusalem 91904, Israel*

(Received 5 October 2019; published 12 December 2019)

Knowledge of the neutron capture of copper and cobalt isotopes is important for the understanding of abundances of the heavier elements produced via the weak *s* process. There are considerable discrepancies for the ^{63}Cu$(n,\gamma)^{64}$Cu and ^{65}Cu$(n,\gamma)^{66}$Cu cross-section values in the literature. New measurements of these cross sections were performed at the SARAF phase I facility using a high-power quasi-Maxwellian neutron source produced by irradiation of the liquid-lithium target (LiLiT) with an intense continuous-wave proton beam. The cross sections were measured by counting the activity of the irradiated targets. The measurement allowed us to evaluate the ^{63}Cu$(n,\gamma)^{64}$Cu, ^{65}Cu$(n,\gamma)^{66}$Cu, and ^{59}Co$(n,\gamma)^{60}$Co Maxwellian averaged cross sections at 30 keV, obtaining values of $70.4 \pm 1.8_{\rm exp} \pm 2.4_{\rm syst}$, $26.8 \pm 1.5_{\rm exp} \pm 1.0_{\rm syst}$, and $38.1 \pm 0.9_{\rm exp} \pm 0.9_{\rm syst}$ mb, respectively. The results are compared with previous measurements in the literature.

DOI: 10.1103/PhysRevC.100.065804

I. INTRODUCTION

The weak slow (*s*) process related to helium burning in massive stars (heavier than eight solar masses) dominates the synthesis of nuclei in the mass range $60 < A < 90$ [1]. In the weak *s*-process regime, the neutron exposure is not high enough to reach equilibrium between the neutron-capture and β-decay rates. In this situation the neutron-capture cross sections of individual isotopes have significant influence on the final abundance distribution of the heavier isotopes up to $A = 90$. The effect on the overall abundance distribution is especially sensitive to the cross sections of the Ni-Cu-Co isotopes, the nuclei at the beginning of the *s*-process path, as demonstrated in Refs. [2,3]. The propagation effect on *s* production of the heavier isotopes was first emphasized for the case of ^{62}Ni [2], where the newly obtained ^{62}Ni$(n,\gamma)^{63}$Ni cross section resulted in an enhancement of 30% of the calculated weak *s* abundances in a wide mass range. A lot of attention was attracted recently to the neutron capture cross section on the copper isotopes. An activation measurement performed in 2008 [3] yielded the ^{63}Cu$(n,\gamma)^{64}$Cu and ^{65}Cu$(n,\gamma)^{66}$Cu Maxwellian averaged cross section (MACS) at 30 keV of $56^{+2.2}_{-5.2}$ and $30^{+1.3}_{-1.9}$ mb, respectively. These values are lower than those recommended in the literature [4,5] (94 ± 10 and 41 ± 5 mb) by ~40% and ~30%, respectively. Such reduction would result in significant decrease in the predicted *s* abundances of the heavier isotopes in the broad range up to $A = 90$ [3]. A novel measurement of the ^{63}Cu$(n,\gamma)^{64}$Cu cross section performed in 2017 via activation and neutron time of flight [6], obtaining the value 84.0 ± 6.8 mb, did not confirm the reduction of the cross section observed in Ref. [3], while the most recent time-of-flight experiment (2019) for measuring the ^{65}Cu$(n,\gamma)^{66}$Cu MACS at 30 keV, 37.0 ± 3.3 mb [7] was in marginal agreement with Ref. [3]. Additional measurements would be beneficial for resolving the discrepancy in the experimental results.

Accurate knowledge of the ^{59}Co$(n,\gamma)^{60}$Co reaction is also important for calculation of the weak *s*-process abundances. This cross section was also measured in Ref. [3], but unlike the case of copper isotopes, there was no discrepancy between the result of this measurement and the recommended value based on previous work [4]. Nonetheless Ref. [3] is the only recent measurement of the ^{59}Co$(n,\gamma)^{60}$Co reaction and an additional measurement is desirable.

A broad experimental program for measuring astrophysical important neutron-induced reactions has been launched at the Soreq Applied Research Accelerator (SARAF) [8] utilizing the intense proton beam and the high-power liquid-lithium target (LiLiT) ([9] and references therein). The ^{7}Li$(p,n)^{7}$Be reaction at proton energy of 1.90–1.94 MeV, just above the reaction threshold 1.88 MeV, has been used as intense neutron sources with energy distributions similar to a Maxwellian distribution at $kT \sim 20$–40 keV. These measurements yield a direct estimations of the MACS needed for the calculation of stellar reaction rates. Bombardment of LiLiT by a 1–2 mA CW (3–4 kW) proton beam allows one to obtain a quasi-Maxwellian neutron source with intensity higher by a factor of ~50 than used in the first-generation experiments of Ref. [10].

We report here on the new measurements of the ^{63}Cu$(n,\gamma)^{64}$Cu[$t_{1/2}$=12.7004(20) h], ^{65}Cu$(n,\gamma)^{66}$Cu[$t_{1/2}$ = 5.120(14) m], and ^{59}Co$(n,\gamma)^{60}$Co[$t_{1/2}$ = 1925.28(14) d] MACS performed at the SARAF phase I facility.

*Corresponding author: weissman@soreq.gov.il

TABLE I. List of the irradiated foils, their properties, and the obtained activation results.

Foil	Purity (%)	Dia. (mm)	Thickness (mg/cm^2)	N_A (atoms)	Produced isotope	Activation at end of irradiation (Bq)	Activation at end of irradiation (atoms)
Gold1	99.9	25	22.51(2)	$3.378(3) \times 10^{20}$	^{198}Au	$4.12(6) \times 10^4$	$1.38(2) \times 10^{10}$
Copper	99.9+	25	11.84(2)	^{63}Cu-$3.807(9) \times 10^{20}$	^{64}Cu	$2.42(2) \times 10^4$	$1.60(1) \times 10^9$
				^{65}Cu-$1.699(9) \times 10^{20}$	^{66}Cu	$1.28(6) \times 10^4$	$5.7(2) \times 10^6$
Gold2	99.9	25	24.24(2)	$3.638(3) \times 10^{20}$	^{198}Au	$4.42(7) \times 10^4$	$1.48(2) \times 10^{10}$
Cobalt	99.5	22	241.31(3)	$9.375(1) \times 10^{21}$	^{60}Co	$1.27(2) \times 10^2$	$3.05(5) \times 10^{10}$
Gold3	99.9	22	25.02(3)	$2.908(3) \times 10^{20}$	^{198}Au	$3.91(6) \times 10^4$	$1.31(2) \times 10^{10}$

II. IRRADIATION AND ACTIVITY MEASUREMENTS

Details about LiLiT irradiation experiments at SARAF were discussed in previous publications [9,11–16]. This irradiation was performed on a new LiLiT apparatus (LiLiT II), which was designed and built according to improved engineering and safety standards. The LiLiT II beam line is installed in a new dedicated target room [8,9] and careful commissioning was performed to ensure good beam transmission. The new setup was benchmarked by repeating activation measurements of the ^{94}Zr$(n,\gamma)^{95}$Zr and ^{96}Zr$(n,\gamma)^{97}$Zr reactions. Very good agreement (<4% relative difference, within quoted uncertainties) was obtained compared to the activation cross sections measured with the first LiLiT target [11], demonstrating full control over the experimental conditions with the new setup.

The lithium target is a windowless film (1.5 mm thick) of liquid lithium at ≈200 °C circulating in a closed loop, serving both for neutron production and as the beam dump and can withstand a few kW of beam power. The beam energy was measured via Rutherford scattering from a thin gold foil and was found to be 1905(5) keV, with an energy spread of 15 keV (1σ). The beam current was monitored by neutron rate measured with a ^{235}U fission chamber (PFC16A, Centronics Ltd.) placed at $0^\circ \approx 70$ cm downstream of the target. A Faraday cup located a meter upstream of the target was used for current calibration. The copper and cobalt foils were irradiated together and sandwiched by gold foils. The latter were used for determination of the neutron fluence via the ^{197}Au$(n,\gamma)^{198}$Au cross section, which is well established in a broad energy range [17,18]. Detailed information of the foils is presented in Table I. The gold1 and gold2 (Table I) foils were used for calibration of the copper foils while gold2 (located between the Cu and Co foil) and gold3 foil were used for calibration of the cobalt foil (see below). The stack of the target foils was placed at the irradiation position approximately 6 mm downstream of the surface of the lithium film. Simulations show that mutual interference of the target stack lead to <0.15% reduction of neutron fluence on either Cu or Co foil.

Starting irradiation with a low-intensity proton beam (duty cycle of 0.5%, obtained by a beam chopper), the beam was ramped up to full intensity by increasing the duty factor, and was kept on target for approximately 6.5 h. The average current was around 0.7 mA. The beam was stable within ±5%; however, a few accelerator trips occurred during irradiation. The calibration of the fission chamber neutron rate against the proton current reading at the Faraday cup was verified again upon end of irradiation. The beam intensity log monitored by the counting rate of the fission chamber was recorded and used later in the activation analysis in order to correct for decay losses during the irradiation. The total beam charge collected on the lithium target was around ≈4.1 mA h, eventually quantified using the Au activation monitor.

The properties of produced isotopes are listed in Table II. After irradiation, the samples were taken out of the irradiation vacuum chamber as soon as the radiation level allowed for entrance to the target room (≈5 min). The prompt extraction of the samples was mostly important because of the relatively short-lived ^{66}Cu isotope. The sample activities were measured using a high-purity shielded Ge (HPGe) detector of 25% relative efficiency from Ortec. The data acquisition of the Ge detector and fission chamber acquisition were synchronized with the accelerator time for careful correction of the decay loss. We conservatively take an uncertainty of 10 s for this synchronization. The efficiency of the detector has been carefully measured with 2% accuracy at different distances in a broad energy range using a number of calibrated γ sources. The targets were measured at known times after the irradiation and different distances from the detector depending on their activity and the half-life of the isotope of interest. The time dependence of the counting rate of the 1039.2 keV and 1345.8 keV γ rays from the copper foil exhibited the decay times corresponding to the ^{66}Cu and ^{64}Cu isotopes, respectively. The activation of the gold and cobalt foils were

TABLE II. The decay properties of the produced isotopes [19–22].

Isotope/Reference	^{198}Au/[19]	^{64}Cu/[20]	^{66}Cu/[21]	^{60}Co/[22]
Half-life	2.6941(2) d	12.7004(20) h	5.120(14) min	1925.28(14) d
γ energy (keV)	411.8	1345.8	1039.2	1173.2 and 1332.5
Branching (%)	95.62(6)	0.4748(34)	9.23(9)	99.85(3) and 99.9836(6)

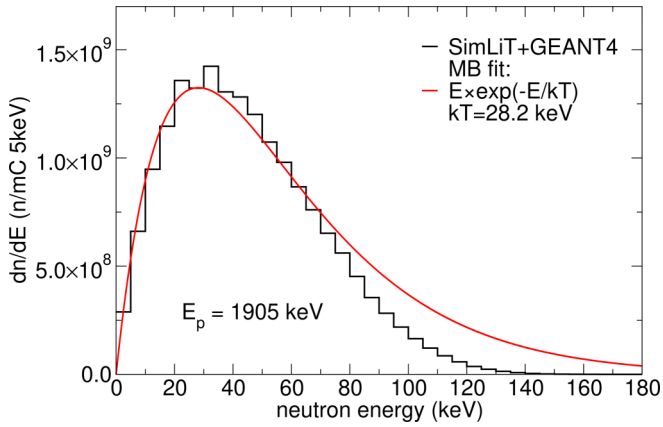

FIG. 1. Simulated neutron spectrum on the targets is compared with fitted MB distribution.

obtained by measuring the counting rate of the 411.8 keV and 1173.2 keV, 1332.5 keV γ rays correspondingly. For all samples, the γ-ray yields were corrected by γ-ray branching ratios, detector efficiency, and decay loss in order to obtain the sample activation and, hence, the number of produced isotope atoms $N_{198\mathrm{Au}}$, $N_{64\mathrm{Cu}}$, $N_{66\mathrm{Cu}}$, and $N_{60\mathrm{Co}}$, at the end of irradiation (see Table I).

III. ANALYSIS AND RESULTS

Detailed description of the analysis and MACS determination can be found in previous publications [9,11–16]. The Monte Carlo simulations performed with the codes SimLiT-GEANT4 [23] included neutron production in the liquid lithium target and neutron transport and scattering in the structural materials and targets. The beam energy and energy spread, as well as the proton beam transverse distribution on the lithium jet, geometrical position of the activation targets, and all surrounding material were introduced into the simulations. The simulated neutron energy distribution spectrum is presented in Fig. 1 together with fitted Maxwell-Boltzman (MB) distribution corresponding to $kT = 28$ keV.

The experimental ^{197}Au cross section, σ_{exp} (Au), was calculated as a convolution of the neutron flux from the SimLiT simulations (dn/dE_n) (Fig. 1) using the ENDF/B-VIII.0 and JENDL-4.0 cross-section evaluations [24,25], both compatible with the most recent time-of-flight capture data [17,18]

$$\sigma_{\mathrm{exp}}(Au) = \int \sigma_{\mathrm{ENDF}}(E_n, Au)\frac{dn}{dE_n}dE_n \Big/ \int \frac{dn}{dE_n}dE_n. \quad (1)$$

Equation (1) yielded σ_{exp}(Au) of 603(12) mb, 602(12) mb, and 591(12) mb for the three gold foils, respectively while using the ENDF/B-VIII.0 library [24]. For consistency, the same cross sections were evaluated using the JENDL-4.0 library [25]. The obtained values are 601(12) mb, 600(12) mb, and 588(12) mb, correspondingly. The cross sections value obtained with the former library were used in the analysis. Uncertainty in evaluation of this cross section was estimated as 2%.

The experimental cross sections for the ^{63}Cu$(n,\gamma)^{64}$Cu, ^{65}Cu$(n,\gamma)^{66}$Cu, and ^{59}Co$(n,\gamma)^{60}$Co reactions, $\sigma_{\mathrm{exp}}(^{63}\mathrm{Cu})$, $\sigma_{\mathrm{exp}}(^{65}\mathrm{Cu})$, and $\sigma_{\mathrm{exp}}(^{59}\mathrm{Co})$, are calculated by Eq. (2):

$$\sigma_{\mathrm{exp}}(X) = \sigma_{\mathrm{exp}}(\mathrm{Au})\frac{N_X}{N_{198\mathrm{Au}}}\frac{N_{\mathrm{Au}}}{N_A}\frac{f_{198\mathrm{Au}}}{f_X}. \quad (2)$$

Where N_{Au} and N_A ($N_{63\mathrm{Cu}}$, $N_{65\mathrm{Cu}}$, or $N_{59\mathrm{Co}}$) are the number of atoms in the respective target foils, while $N_{198\mathrm{Au}}$ and N_X ($N_{64\mathrm{Cu}}/N_{66\mathrm{Cu}}/N_{60\mathrm{Co}}$) are the number of nuclei produced in the corresponding targets foils by end of irradiation (Table I). The factors $f_{198\mathrm{Au}}$ and f_x in Eq. (2) reflect the decay losses during the irradiation for ^{198}Au and X (^{64}Cu, ^{66}Cu, or ^{60}Co) isotopes respectively. Variation of the beam current and, hence, the neutron rate during the irradiation was taken into account in the calculations of the $f_{198\mathrm{Au}}$ and f_x factors.

The budget of experimental uncertainties in the cross section values is presented in Table III. Note that the effective uncertainty of HPGe γ-detection efficiency is lower than the 2% uncertainty quoted above. This is due to the relative character of measurement of the photopeaks of interest with respect to the gold 411.8 keV activation γ line. Uncertainty for decay losses in the case of ^{66}Cu is associated with the short half-time of this nuclei. The obtained values of $\sigma_{\mathrm{exp}}(^{63}\mathrm{Cu})$, $\sigma_{\mathrm{exp}}(^{65}\mathrm{Cu})$, and $\sigma_{\mathrm{exp}}(^{60}\mathrm{Co})$ were found to be 72.8(19) mb, 28.0(15) mb, and 37.9(9) mb (Table IV).

Contribution to the ^{64}Cu activity from the ^{65}Cu$(\gamma,n)^{64}$Cu reaction due to high-energy γ rays (14.6, 17.6 MeV) emitted by the ^{7}Li$(p,\gamma)^{8}$Be reaction [11] was calculated using experimental values of the ^{65}Cu$(\gamma,n)^{64}$Cu cross section [26]

TABLE III. Summary of the experimental uncertainties in determination of σ_{exp}.

Source of uncertainty	$\sigma_{\mathrm{exp}}(^{63}\mathrm{Cu})$ Uncertainty (%)	$\sigma_{\mathrm{exp}}(^{65}\mathrm{Cu})$ Uncertainty (%)	$\sigma_{\mathrm{exp}}(^{59}\mathrm{Co})$ Uncertainty (%)
σ_{exp} (Au) evaluation	2	2	2
$N_{198\mathrm{Au}}$ (stat. error)	0.3	0.3	0.3
N_{Au} (foil weighting)	0.1	0.1	0.1
HPGe eff. rel. to 411.8 keV Au photopeak	1.0	1.0	1.0
Statistical unc. in gamma peak	1.1	4.3	0.3
Uncertainty N_X (foil weighting)	0.1	0.1	0.1
Estimation of the decay loss	0.2	2.3	<0.1
γ-ray intensity	0.7	1.0	<0.1
Total uncertainty	2.6	5.5	2.3

TABLE IV. The MACS cross section calculated from the experimental cross sections using ENDF/B-VIII.0, JENDL-4.0, JEFF-3.3, and TENDL-2017 nuclear libraries [24,25,27,28]. All $C_{lib}(A)$ and $\sigma^{lib}_{MACS}(A)$ values were calculated for $kT = 30$ keV.

	^{63}Cu	^{65}Cu	^{59}Co
$\sigma_{exp}(A)/\sigma_{exp}(Au)$	0.121(3)	$4.6(3) \times 10^{-2}$	$6.36(4) \times 10^{-2}$
$\sigma_{exp}(A)$ (mb)	72.8(19)	28.0(15)	37.9(9)
$C_{ENDF}(A)$	0.95	0.89	0.92
$C_{JENDL}(A)$	0.89	0.88	0.86
$C_{JEFF}(A)$	0.86	0.88	0.92
$C_{TENDL}(A)$	0.86	0.85	0.89
$\sigma^{ENDF}_{MACS}(A)$ (mb)	$78.3 \pm 2.1_{exp} \pm 0.8_{syst}$	$28.1 \pm 1.5_{exp} \pm 0.7_{syst}$	$39.2 \pm 0.9_{exp} \pm 0.7_{syst}$
$\sigma^{JENDL}_{MACS}(A)$ (mb)	$72.9 \pm 1.9_{exp} \pm 1.9_{syst}$	$27.9 \pm 1.5_{exp} \pm 0.7_{syst}$	$36.8 \pm 0.8_{exp} \pm 1.2_{syst}$
$\sigma^{JEFF}_{MACS}(A)$ (mb)	$70.6 \pm 1.9_{exp} \pm 2.3_{syst}$	$27.9 \pm 1.5_{exp} \pm 0.8_{syst}$	$39.4 \pm 0.9_{exp} \pm 0.7_{syst}$
$\sigma^{TENDL}_{MACS}(A)$(mb)	**$70.4 \pm 1.8_{exp} \pm 2.4_{syst}$**	**$26.8 \pm 1.5_{exp} \pm 1.0_{syst}$**	**$38.1 \pm 0.9_{exp} \pm 0.9_{syst}$**

and found to be negligible compared to the measured ^{64}Cu production [$1.60(1) \times 10^9$, Table I)].

The quasi-Maxwellian neutron energy spectrum used in the irradiation differs, mainly in the high-energy tail, from a pure MB distribution (Fig. 1). Extrapolation of the experimental cross section, $\sigma_{exp}(X)$ to the MACS cross section, $\sigma_{MACS}(X, kT)$ requires a correction, which was obtained using the evaluated cross sections from nuclear libraries. The MACS cross section is obtained from the experimental cross section from ratios of the integrations of the evaluated cross section, $\sigma_{lib}(X, E_n)$ over MB and simulated, dn/dE_n, distributions (see Ref. [11] for details):

$$\sigma_{MACS}(A, kT) = \frac{2}{\sqrt{\pi}}\sigma_{exp}(A) \times C_{lib}(A, kT), \tag{3}$$

where

$$C_{lib}(A, kT) = \frac{\int_0^\infty \sigma_{lib}(A, E_n) E_n e^{-E_n/kT} dE_n}{\int_0^\infty E_n e^{-E_n/kT} dE_n} \times \frac{\int_0^\infty \frac{dn}{dE_n} dE_n}{\int_0^\infty \sigma_{lib}(A, E_n) \frac{dn}{dE_n} dE_n}. \tag{4}$$

The results for C_{lib} calculated for $kT = 30$ keV, using the most updated versions of four nuclear libraries, ENDF/B-VIII.0, JENDL-4.0, JEFF-3.3, and TENDL-2017 [24,25,27,28] are presented in Table IV. As can be seen in the table, there is some scattering in the calculated correction factors, C_{lib}. It was demonstrated in Ref. [6] that the TENDL library provides the best agreement with the experimental MACS results for the case of ^{63}Cu$(n, \gamma)^{64}$Cu. We adopted here the final MACS cross section corrected using the most recent version of TENDL library, TENDL-2017. The σ_{MACS} cross sections obtained with other libraries are also shown in Table IV for sake of completeness. The second uncertainty (systematic uncertainty) in the quoted σ_{MACS} reflects the uncertainty associated with library correction in MACS calculations. This uncertainty was estimated conservatively as 20% of the correction factor, $(0.2 \times |1 - C_{lib}|)$.

IV. DISCUSSION

The recent chapter in measuring these processes started in 2008, when Heil *et al.* [3] obtained a value of MACS by activation using a quasistellar neutron source at Karlsruhe. The ^{63}Cu$(n, \gamma)^{64}$Cu, ^{65}Cu$(n, \gamma)^{66}$Cu MACS measured in Ref. [3] were significantly lower than the results of the earlier work of Panday *et al.* [4]. Such a reduction in the cross sections would result in a decrease of 20% of the isotopes yields in the broad range $60 \leqslant A \leqslant 90$. It is worth mentioning that the MACS for the ^{59}Co$(n, \gamma)^{60}$Co obtained in Ref. [3] is in very good agreement with the early work of Spencer *et al.* in 1976 [29].

The results of Ref. [3] sparked interest to the ^{63}Cu$(n, \gamma)^{64}$Cu, ^{65}Cu$(n, \gamma)^{66}$Cu cross sections. Two experiments [6,7], were performed very recently to measure the cross sections. The ^{63}Cu$(n, \gamma)^{64}$Cu MACS was measured in Ref. [6] via activation using a quasistellar neutron source at JRC, Geel. In the same work, the excitation function was measured with the time-of-flight technique. The ^{65}Cu$(n, \gamma)^{66}$Cu MACS was determined at LANL [7] using the time-of-flight technique. The results obtained

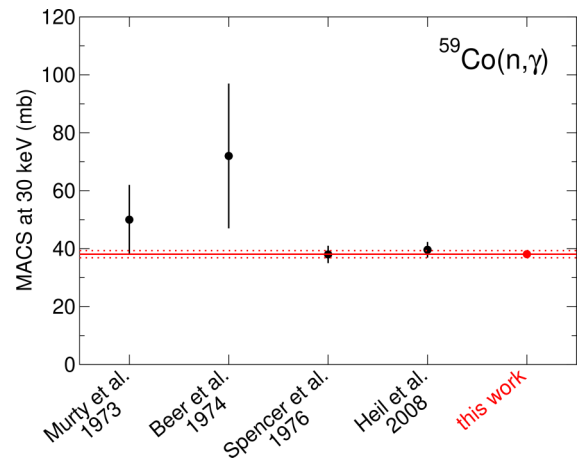

FIG. 2. Comparison of the obtained 30 keV $\sigma_{MACS}(^{59}Co)$ with the previous experiments [3,29–31].

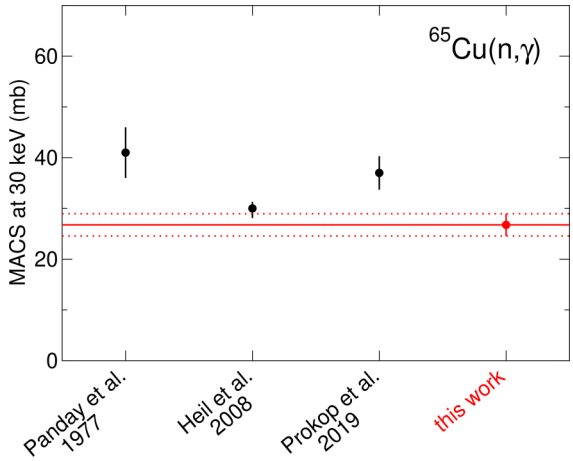

FIG. 3. Comparison of the obtained 30 keV $\sigma_{\mathrm{MACS}}(^{65}\mathrm{Cu})$ with the previous experiments [3,4,7].

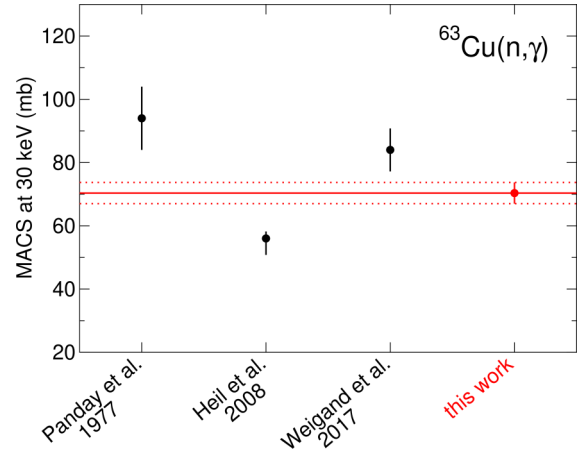

FIG. 4. Comparison of the obtained 30 keV $\sigma_{\mathrm{MACS}}(^{63}\mathrm{Cu})$ with the previous experiments [3,4,6]. The MACS for Panday *et al.* [4] was calculated by Ref. [5].

for the ^{63}Cu$(n,\gamma)^{64}$Cu, ^{65}Cu$(n,\gamma)^{66}$Cu cross sections [6,7] were higher than those of Ref. [3] by 50% and 23%, correspondingly, thus undermining the astrophysical implications of the latter work.

The main goal of the present work was to improve the experimental knowledge of the copper cross sections and to attempt resolving the controversy existing in the literature. It was suggested in Ref. [6] that the reason for the reduced cross section in Ref. [3] was the 1 mm thick copper backing of metallic lithium target used for neutron production. It was argued that the copper backing resulted in significant modification of the neutron spectrum and the overall neutron flux. In the case of LiLiT the only material between the sample and the source are a 0.35 mm thick stainless steel (SS) foil supporting the lithium jet and a 0.65 mm thick SS wall between the LiLiT vacuum chamber and the irradiation chamber. The effect of this material on the neutron spectrum is much smaller due to the lower scattering cross section. In addition, all the materials surrounding the LiLiT target were carefully included into the SimLiT-GEANT4 simulations (Fig. 1). Therefore, measurements at LiLiT are less prone to systematic uncertainty. Measurement of the three cross sections simultaneously performed in this work could be beneficial as it provides more direct comparison with the literature. For instance, the ^{59}Co$(n,\gamma)^{60}$Co MACS could serve as a good cross check of different experiments.

The summary of the experimental results for the ^{63}Cu$(n,\gamma)^{64}$Cu, ^{65}Cu$(n,\gamma)^{66}$Cu, and ^{59}Co$(n,\gamma)^{60}$Co MACS are presented in Figs. 2–4. As can be seen from the figures, the present $\sigma_{\mathrm{MACS}}(^{59}\mathrm{Co})$ measurement is in perfect agreement with Ref. [3] (Fig. 2). The results of the two measurements [3,4] are also in reasonable agreement for $\sigma_{\mathrm{MACS}}(^{65}\mathrm{Cu})$, while the time-of-flight experiment [7] yields a higher cross section (Fig. 3). However, our measurement of $\sigma_{\mathrm{MACS}}(^{63}\mathrm{Cu})$ yields the value in between the results of the two activation experiments [3,6].

It is difficult to comment on the overall situation presented in Fig. 2–4. The present work somewhat improved but not elucidated completely the discrepancy in the literature. Most likely there are additional systematic errors in some experiments, which were not properly accounted for.

In conclusion, careful measurements of the ^{63}Cu$(n,\gamma)^{64}$Cu, ^{65}Cu$(n,\gamma)^{66}$Cu, and ^{59}Co$(n,\gamma)^{60}$Co Maxwellian averaged cross sections at 30 keV were performed at SARAF phase I using the new version of the LiLiT target. The obtained MACS values are $70.4 \pm 1.8_{\mathrm{exp}} \pm 2.4_{\mathrm{syst}}$, $26.8 \pm 1.5_{\mathrm{exp}} \pm 1.0_{\mathrm{syst}}$, and $38.1 \pm 0.9_{\mathrm{exp}} \pm 0.9_{\mathrm{syst}}$ mb, respectively, where the quoted systematic uncertainties are the conservatively estimated errors of the Maxwell-Boltzmann corrections obtained with the TENDL-2017 library. The new results are essential for improvement of the astrophysical network calculations used for calculation of the isotope abundances generated via the weak *s* process.

ACKNOWLEDGMENT

We are grateful to D. Berkovits for his comments to this paper. We gratefully acknowledge the support of the Pazy Foundation (Israel).

[1] H. Beer, G. Walter, and F. Kappeler, Astrophys. J. **389**, 784 (1992).
[2] H. Nassar *et al.*, Phys. Rev. Lett. **94**, 092504 (2005).
[3] M. Heil, F. Käppeler, E. Ubersender, R. Gallino, and M. Pignatari, Phys. Rev. C **77**, 015808 (2008).
[4] M. S. Pandey, J. B. Garg, and J. A. Harvey, Phys. Rev. C **15**, 600 (1977).
[5] Z. Y. Bao, H. Beer, F. Käppeler, F. Voss, K. Wisshak, T. Rauscher, and I. Dillmann, AIP Conf. Proc. **819**, 132 (2006); online at: http://www.kadonis.org.
[6] M. Weigand *et al.*, Phys. Rev. C **95**, 015808 (2017).

[7] C. J. Prokop, A. Couture, S. Jones, S. Mosby, G. Rusev, J. Ullmann, and M. Krtička, Phys. Rev. C **99**, 055809 (2019).
[8] I. Mardor *et al.*, Eur. Phys. J. A **54**, 91 (2018).
[9] M. Paul *et al.*, Eur. Phys. J. A **55**, 44 (2019).
[10] W. Ratynski and F. Kappeler, Phys. Rev. C **37**, 595 (1988).
[11] M. Tessler *et al.*, Phys. Lett. B **751**, 418 (2015).
[12] L. Weissman *et al.*, Phys. Rev. C **96**, 015802 (2017).
[13] A. Shor *et al.*, Phys. Rev. C **96**, 055805 (2017).
[14] S. Pavetich *et al.*, Phys. Rev. C **99**, 015801 (2019).
[15] M. Tessler *et al.*, Phys. Rev. Lett. **121**, 112701 (2018).
[16] C. Guerrero *et al.*, Phys. Lett. B **797**, 134809 (2019).
[17] C. Lederer *et al.*, Phys. Rev. C **83**, 034608 (2011).
[18] C. Massimi *et al.*, Eur. Phys. J. A **50**, 124 (2014).
[19] H. Xiaolong and K. Mengxiao, Nucl. Data Sheets **133**, 221 (2016).
[20] M.-M. Be *et al.*, Appl. Rad. and Isotopes, **70**, 1894 (2012).
[21] E. Browne and J. K. Tuli, Nucl. Data Sheets **111**, 1093 (2010).
[22] E. Brown and J. K. Tuli, Nucl. Data Sheets **114**, 1849 (2013).
[23] M. Friedman *et al.*, Nucl. Instr. and Meth. A **698**, 117 (2013).
[24] D. A. Brown *et al.*, Nucl. Data Sheets **148**, 1 (2018).
[25] K. Shibata *et al.*, J. Nucl. Sci. Technol. **48**, 1 (2011).
[26] R. A. Alvarez, B. L. Berman, D. D. Faul, F. H. Lewis, Jr., and P. Meyer, Phys. Rev. C **20**, 128 (1979).
[27] JEFF-3.3 Library, Joint Evaluated Fission and Fusion, https://www.oecd-nea.org/dbdata/jeff/jeff33/index.html, 2017.
[28] A. J. Koning *et al.*, TENDL-2017, https://tendl.web.psi.ch/tendl_2017/tendl2017.html, 2017.
[29] R. R. Spencer and R. L. Macklin, Nucl. Sci. Eng. **61**, 346 (1976).
[30] M. S. Murty, K. Siddappa, and J. Rama Rao, J. Phys. Soc. Jpn. **35**, 8 (1973).
[31] H. Beer, R. R. Spencer, and A. Ernst, Astron. Astrophys. **37**, 197 (1974).